Front. Struct. Civ. Eng. 2024, 18(10): 1479–1491
https://doi.org/10.1007/s11709-024-1065-3

RESEARCH ARTICLE

Investigation on identification of structural anomalies from polluted data sets using an unsupervised learning method

Junchen YE[a], Zhixin ZHANG[b], Ke CHENG[b], Xuyan TAN[c,d], Bowen DU[a*], Weizhong CHEN[c,d]

[a] *School of Transportation Science and Engineering, Beihang University, Beijing 100191, China*
[b] *CCSE Lab, Beihang University, Beijing 100191, China*
[c] *State Key Laboratory of Geomechanics and Geotechnical Engineering, Institute of Rock and Soil Mechanics Chinese Academy of Sciences, Wuhan 430071, China*
[d] *University of Chinese Academy of Sciences, Beijing 100049, China*
[*] *Corresponding author. E-mail: dubowen@buaa.edu.cn*

ABSTRACT Civil infrastructure is prone to structural damage due to high geo-stress and other natural disasters, so monitoring is required. Data collected by structural health monitoring (SHM) systems are easily affected by many factors, such as temperature, sensor fluctuation, sensor failure, which can introduce a lot of noise, increasing the difficulty of structural anomaly identification. To address this problem, this paper designs a new process of structural anomaly identification under noisy conditions and offers Civil Infrastructure Denoising Autoencoder (CIDAE), a denoising autoencoder-based deep learning model for SHM of civil infrastructure. As a case study, the effectiveness of the proposed model is verified by experiments on deformation stress data of the Wuhan Yangtze River Tunnel based on finite element simulation. Investigation of the circumferential weld and longitudinal weld data of the case study is also conducted. It is concluded that CIDAE is superior to traditional methods.

KEYWORDS structural health monitoring, deep learning, anomaly detection

1 Introduction

Civil infrastructure is exposed to complex geological conditions and may encounter various natural disasters, which make it prone to exhibit structural damage [1–3]. Therefore, it is of great significance to conduct health detection on the abnormal state of civil infrastructure [4].

Structural health monitoring (SHM) is a hot and developing research field. The massive data collected by SHM system provides the basis for damage assessment of engineering structures [5]. In general, anomaly detection methods based on SHM data can be divided into model-driven and data-driven methods [6]. Cao et al. [7] developed a piezoelectric impedance measurement for structural damage identification by inverse analysis. Moore et al. [8] identified cracks in thin plates by model updating. Xu et al. [9] proposed a two-step model-driven approach to accurately characterize and continuously monitor fatigue damage. Model-driven methods need to construct specific models for different infrastructure structures, and cannot comprehensively consider various factors that lead to anomalies, which make them difficult to apply [10]. An alternative to a model-driven method is a data-driven method. Some statistical approaches based on SHM data inherently take uncertainties into account and do not rely on physical models, which makes them more suitable for automated SHM systems than model-driven approaches. A statistical pattern recognition-based method called the vector autoregressive moving average model has been proposed to identify damage locations in an idealized steel bridge girder [11]. To reduce manual analysis, Chen et al. [3] proposed a dynamic warning method based on integrated autore-gressive moving average model which integrates differencing to stabilize

Article history: Received Apr 17, 2023; Accepted Sep 2, 2023

non-stationary data for predicting future values and verified the effectiveness of the model by conducting experiments on the concrete strain data of the Hong Kong−Zhuhai−Macao, China, Bridge immersed tunnel. Xiao et al. [12] proposed an analysis method based on the least square support vector machine to establish a complex nonlinear failure criterion via iteration computation based on strength test data of the soil, and this method is of extensive applicability to many problems of slope stability.

In recent years, machine learning (ML) methods have attracted the attention of many researchers in the field of SHM [13]. Sheikh Khozani et al. [14] used a set of data mining and machine learning algorithms including Random Forest, M5P, Random Committee, KStar and Additive Regression, implemented on attained data to predict the shear stress distribution in a compound channel which is various types of data in SHM. Mai et al. [15] developed different ML models for predicting the compressive strength of fiber-reinforced self-compacting concrete to address these limitations. ML algorithms can be broadly classified into supervised and unsupervised learning algorithms. Due to non-requirement of abnormal labels to guide model training, unsupervised learning algorithms have the broadest application scenarios [16]. Autoencoder (AE) and its variants that can process time series are widely used in anomaly detection [17,18]. Moallemi et al. [19] proposed three compression models, namely a Principal Component Analysis (PCA), a fully-connected AE, and a convolutional AE, for anomaly identification in bridge structures. To detect the temporal and spatial anomalies of a dam, Shu et al. [20] proposed a novel spatial-temporal variational AE consisting of a recurrent neural network and a graph convolutional network. A Convolutional Neural Network (CNN) which can assign importance (learnable weights and biases) to various objects can also be used for anomaly detection. Cha et al. [21] proposed a vision-based method using a deep architecture of CNNs for detecting concrete cracks without calculating defect features. Chiaia et al. [22] proposed a multi-level strategy based on CNNs, designed and implemented on the basis of periodic structural monitoring that was oriented to a cost- and time-efficient tunnel control plan. To provide quasi real-time simultaneous detection of multiple types of damages, a Faster Region-based Convolutional Neural Network (Faster R-CNN)-based structural visual inspection method is proposed. But few of these studies take into account the noise widely existing in real situations. In fact, civil infrastructure is generally in a complex environment, and the data collected by SHM system is often affected by temperature, humidity, sensor performance degradation, sensor fluctuations and other uncontrollable external factors, which makes SHM system data full of noise [23]. The noise makes the data distribution exhibit more nonlinearities and complexities, which further increases the difficulty of anomaly detection and easily activates false alarms [24]. Since real infrastructure structural anomaly data are difficult to obtain, a simulated 12-story building model and a laboratory-scaled steel bridge was designed and fabricated by the Steel Bridge Design Team of the University of Manitoba [16]. Wang and Cha [25] studied the infrastructure structure anomaly detection by means of unsupervised learning, and proposed an unsupervised deep learning method based on a deep auto-encoder with a one-class support vector machine. The validity of the model is verified based on physical model data containing noise. Cha and Wang [26] also proposed a new structural damage detection and localization method using a density-peaks-based fast clustering algorithm. They used a Gaussian radius kernel function and continuous wavelet transform to improve the performance of the algorithm. Favarelli et al. [27] studied the effect of measurement noise on bridge damage detection. Yan et al. [28] proposed a hybrid robust convolutional AE for machine tool anomaly detection under noise. Active noise control/cancelation is a method to reduce the impact of noise. The following work utilizes this method. Mostafavi and Cha [29] proposed a novel high-performance deep-learning-based feedforward active noise reduction (ANC) controller to attenuate construction-related noise by considering the delay and nonlinear behavior of acoustic devices. In addition, an advanced deep learning-based feedback ANC named DNoiseNet [30] has also been proposed to overcome the limitations of traditional ANCs and learn multilevel temporal features under different noises in various environments. Some analytical methods based on statistical knowledge and mathematical derivation have been applied to the problem of anomaly detection under strong noise [31,32]. However, there is little research on anomaly detection under general noisy conditions.

This paper proposes an anomaly detection model named Civil Infrastructure Denoising Autoencoder (CIDAE) to identify civil infrastructure anomalies in noisy environments. This method employs an unsupervised learning framework to adapt to the problem of unknown anomaly labels in real scenes. CIDAE is based on the AE structure, and a denoising reduction mechanism is designed to accommodate the effect of noise on the data distribution. CIDAE is used to extract a robust representation of normal data, which is not affected by noise and abnormal data, and contains the essential characteristics of normal data. Experiments are conducted on the deformation stress data set of the Wuhan Yangtze River Tunnel based on finite element simulation to verify the effectiveness of the proposed model.

The sections are organized as follows. Section 2 lists

the definition of anomaly detection and the parameters used in this article. Section 3 introduces the proposed model. Section 4 presents the construction process of the finite element simulation data set. Section 5 and Section 6 introduce the experiments and comparison experiments based on the finite element simulation data set, with Subsection 6.3 providing a case study to discuss the performance of the model on a real data set. Section 7 presents the conclusions and possible future research directions.

2 Preliminaries for structural anomaly identification

This section aims to formalize the problem of structural anomaly identification in the field of civil engineering. Some of the definitions in our anomaly detection model are introduced first, and then the formalization of the time series anomaly detection task subjected to noise pollution is provided.

2.1 Definition of model parameter

The anomaly identification model is a crucial form to express information, and is established based on monitoring information. The main parameters used to develop our proposed model are defined as follows.

Sample. a sample refers to an individual data point in a data set used for training a model. A notation x_t^i represents the data recorded by sensor i at time t. The number of sensors is denoted as I.

Time series. Data recorded by a sensor at equal intervals over a period of time constitute a time series. We use $\mathcal{T}^i = \{x_1^i, x_2^i, \ldots, x_T^i\}$ to represent time series constituted by data which are recorded by sensor i, and the length of $\mathcal{T}^i$ is T.

Sliding window. Considering the dependencies between time series data, the original time series is usually split into a sequence of sliding windows and then fed into the anomaly detection model. Consecutive W samples on a time series recorded by sensor i constitute a sliding window $w_k^i = \{x_k^i, x_{k+1}^i, \ldots, x_{k+W}^i\}$, $\{k = 1, 2, \ldots, T - W\}$, W is the window size, so a time series is transformed into $W^i = \{w_1^i, w_2^i, \ldots, w_{T-W}^i\}$, and we use $\mathbb{W} = \{\mathcal{W}^1, \mathcal{W}^2, \ldots, \mathcal{W}^I\}$ to denote the set of all sliding windows.

Reconstruction. After the original data, $\mathbb{W} = \{\mathcal{W}^1, \mathcal{W}^2, \ldots, \mathcal{W}^I\}$ is put into the anomaly detection model, the hidden layer representation $\mathbb{H} = \{\mathcal{H}^1, \mathcal{H}^2, \ldots, \mathcal{H}^I\}$ can be obtained. Here $\mathcal{H}^i = \{h_1^i, h_2^i, \ldots, h_{T-W}^i\}$ where h_T^i indicates the hidden states on the Tth time step of i-th layer. Then, the input data can be reconstructed as $\tilde{\mathbb{W}} = \{\tilde{\mathcal{W}}^1, \tilde{\mathcal{W}}^2, \ldots, \tilde{\mathcal{W}}^I\}$, $\tilde{\mathcal{W}}^i = \{\tilde{w}_1^i, \tilde{w}_2^i, \ldots, \tilde{w}_{T-W}^i\}$, $\tilde{\mathrm{w}}_k^i = \{\tilde{x}_k^i, \tilde{x}_{k+1}^i, \ldots, \tilde{x}_{k+W}^i\}$. The distance between the original data x_t^i and the reconstructed one $\tilde{x}_t^i$ can be defined as $d_t^i = \|x_t^i - \tilde{x}_t^i\|$.

2.2 Formalization of anomaly identification

Anomaly identification is a process that reconstructs a series or a matrix from its transformed counterpart, and can then calculate the discrepancy between reconstructed results and original data. Given a matrix $\mathbb{T}$, which consists of a multiple time series, $\mathbb{T} = \{\mathcal{T}^1, \mathcal{T}^2, \ldots, \mathcal{T}^I\}$. The objective of traditional anomaly detection model is to distinguish a label $y_t^i = \{0, 1\}$ for each sample x_t^i, where 0 indicates normal and 1 indicates anomaly. Differently from the traditional anomaly detection, in the case of anomaly detection with noise pollution, we set label y_t^i to have three possible values, $y_t^i = \{0, 1, 2\}$, where 0 indicates normal, 1 indicates real anomaly, and 2 indicates a sample with abnormal representation but is actually noise. A sequence of sliding windows $\mathbb{W} = \{\mathcal{W}^1, \mathcal{W}^2, \ldots, \mathcal{W}^I\}$ are fed into the anomaly identification model to reconstruct $\tilde{\mathbb{W}} = \{\tilde{\mathcal{W}}^1, \tilde{\mathcal{W}}^2, \ldots, \tilde{\mathcal{W}}^I\}$. If the reconstruction error d_t^i of sample x_t^i is larger than threshold, then sample x_t^i will be considered to present an anomaly.

3 Methodology

This section presents the general framework of anomaly detection and the implementation process and details of CIDAE. The diagram flow of anomaly detection is shown in Fig. 1. After preprocessing, the training set data is used to train the model, and then the compressed features of the validation set data are input into the Gaussian distribution model to obtain the anomaly threshold. Finally, the trained model and the anomaly threshold are used to test the effectiveness of the proposed model on the testing set.

3.1 Overview of the proposed model

The architecture of the proposed model is displayed in Fig. 1. As shown in this figure, the model we proposed to resolve the anomaly detection problem with noise pollution is based on AE. What the encoder and decoder need to do is to map the feature space vector into hidden space and then reconstruct the hidden space vector back into the feature space. After adding disturbance to the original time series, the corrupted data will be processed into the form of the sliding window, and then be fed into the AE. The distance between the clean data and the reconstructed data will be calculated. Finally, by setting a threshold, the reconstruction error can be used to determine whether the sample is abnormal or not.

3.2 The traditional AutoEncoder

AE is an artificial neural network based on unsupervised learning. We design the encoder and the decoder as

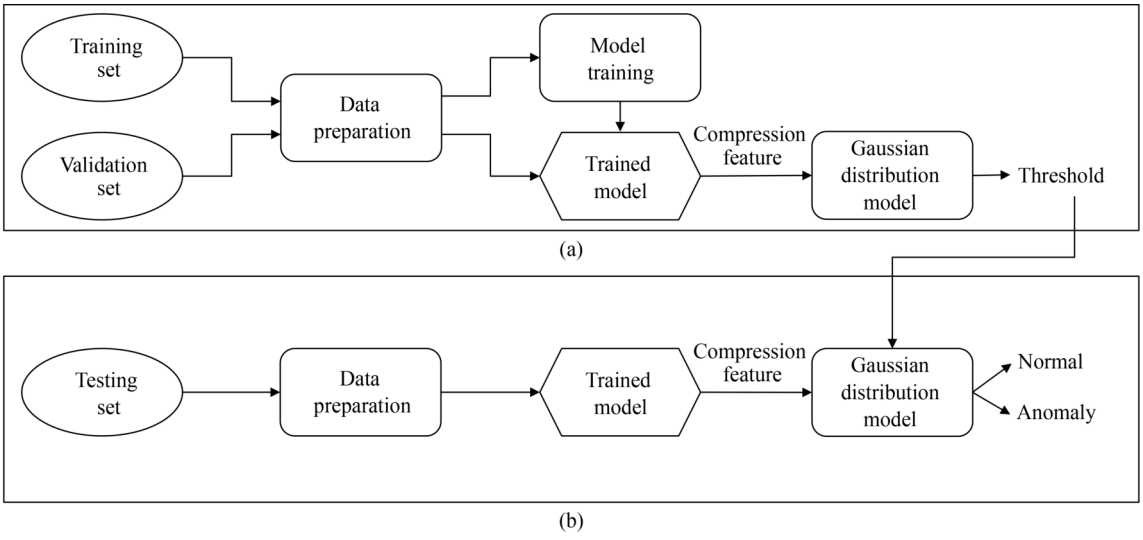

Fig. 1 The diagram flow of anomaly detection: (a) training process; (b) testing process.

structures consisting of long short term memory (LSTM) layers. The calculation process of LSTM is shown in the following equations:

$$i_t = \sigma(K_{\mathrm{i}} \times [\boldsymbol{h}'_{t-1}, x_t] + b_{\mathrm{i}}), \tag{1}$$

$$f_t = \sigma(K_{\mathrm{f}} \times [\boldsymbol{h}'_{t-1}, x_t] + b_{\mathrm{f}}), \tag{2}$$

$$o_t = \sigma(K_{\mathrm{o}} \times [\boldsymbol{h}'_{t-1}, x_t] + b_{\mathrm{o}}), \tag{3}$$

$$\tilde{C}_t = \tanh(K_{\mathrm{C}} \times [\boldsymbol{h}'_{t-1}, x_t] + b_{\mathrm{C}}), \tag{4}$$

$$C_t = f_t \times C_{t-1} + i_t \times \tilde{C}_t, \tag{5}$$

$$\boldsymbol{h}'_t = o_t \times \tanh C_t, \tag{6}$$

where $\boldsymbol{h}'_t$ is the hidden layer vector at time t; $\boldsymbol{h}'_{t-1}$ is the hidden layer vector at the previous time; x_t is the input at time t; K_{i}, K_{f}, K_{o}, and K_{C} are the weight matrices; b_{i}, b_{f}, b_{o}, and b_{C} are the bias; C_t represents long-term memory. The encoder transforms the input matrix $X \in \mathbb{R}^{N \times W \times F}$ into a hidden vector $\boldsymbol{H} \in \mathbb{R}^{N \times W \times D}$, where F represents the feature dimension of the original data, N is the number of sliding windows, W is the size of the sliding window, and D is the feature dimension of the hidden vector. The decoder does the opposite. By taking the input information as the learning target, AE can learn a representation of the input data.

3.3 The denoising AutoEncoder

A traditional AE can map the inputs to useful intermediate representations that contain characteristic information about the inputs during the reconstruction process. However, due to the influence of model complexity, data volume, data noise and other problems, the learning process of AE often has the risk of overfitting. In an anomaly detection scenario, the input data may contain both normal data and abnormal data, and the data may be contaminated by noise. The overfitting problem will significantly reduce the ability of the model to detect anomalies accurately. Therefore, we need to learn a more robust intermediate representation that is free from noise and abnormal data, and contains essential features of normal data.

Vincent et al. [33] hypothesize and investigate an additional specific criterion: robustness to partial destruction of the input. That is, partially destroyed inputs should yield almost the same representation. Inspired by this work, we design a Denoising AutoEncoder (DAE) to learn intermediate representations of the input data. As Fig. 2 shows, we add noise ϵ to the input data. Using $\hat{X}$ to represent the data after adding noise, H is the hidden state vector, and the calculation process of the encoder and decoder can be expressed as

$$f_{\mathrm{enc}} : H = RNN\left(\hat{X}\right), \tag{7}$$

$$f_{\mathrm{dec}} : \tilde{X} = RNN(H).$$

Unlike basic AE, CIDAE hopes to learn clean data representations from corrupted data. So the reconstruction error of CIDAE can be expressed as

$$L_{\mathrm{rec}} = \frac{1}{N} \sum_{w=1}^{W} \|\mathrm{x}_w - \tilde{\mathrm{x}}_w\|, \tag{8}$$

where L_{rec} is the reconstruction error. We also use the reconstruction error as the objective function.

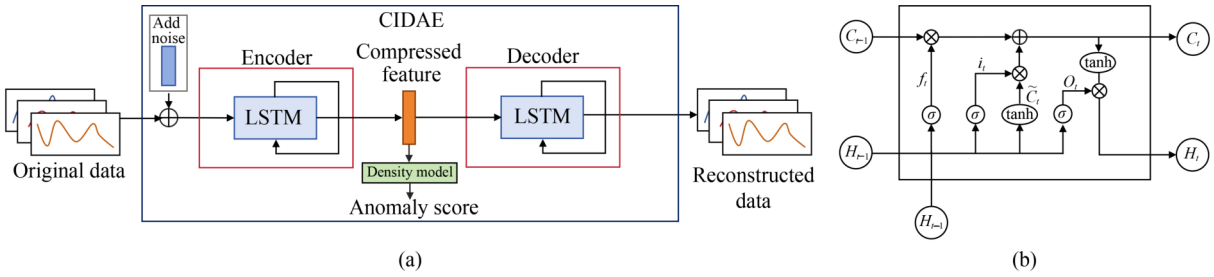

Fig. 2 Framework of the anomaly detection model: (a) the structure of CIDAE; (b) a LSTM unit.

3.4 Detection procedure

After the model is trained, CIDAE learns a sufficiently robust intermediate representation of the original data. The hidden state vector contains enough characteristic information of the original data. We use a multivariate Gaussian distribution model to determine whether the observation is abnormal. The probability density function of the multivariate Gaussian distribution model can be expressed as

$$\text{Gauss}(H) = \frac{1}{\left(\sqrt{2\pi}\right)^{D}\prod_{k=1}^{D}\sigma_k} e^{-\sum_{k=1}^{D}\frac{(h_k-\mu_k)^2}{2\sigma_k^2}}, \qquad (9)$$

where D is the feature dimension of the hidden state vector, h_k is the kth dimension of the hidden layer vector, σ_k and μ_k are the standard deviation and the mean value of hidden state vector on dimension k. Taking the required data into the above equation, we can obtain the probability of each observation. Observations with probability less than the threshold are considered as anomalies.

4 Data information

Some researchers simulate the process of infrastructure deformation based on physical experiments and verify the validity of the model based on such data. But physical experiments are expensive and involve a lot of uncontrollable factors. Therefore, this paper constructs a numerical model of the tunnel based on the finite element simulation method, and then applies the concentrated forces in a certain location in the tunnel to simulate the deformation process of the tunnel. The numerical simulation process and the finite element simulation data are introduced in this section.

4.1 Development of a tunnel numerical model

A numerical model of tunnel structure is developed on the basis of the finite element method. The experimental data can be obtained by applying different boundary conditions to the developed model. According to the background of an underwater shield tunnel located in Wuhan, China [34], the numerical model with five rings, as shown in Fig. 3, is developed. The external and internal diameters of this tunnel are 11 and 10 m, respectively. In addition, each ring consists of 9 concrete segments with bolt connection, including one key segment, two adjacent segments, and six standard segments.

The numerical model of the tunnel structure is separated into tetrahedral elements for calculation and different material properties are assigned to concrete segment and connected bolts. Specifically, the segment material is C60 concrete, and the bolt is steel. The main parameters of these materials are given in Table 1. To simulate the plastic behavior of tunnel structure, the stress–strain relation of concrete is provided in Table 2, which is also assigned on the material property.

In the simulation phase, the rotational freedoms in all directions are constrained, and contact pairs of tie are applied to bolt and nuts and surface-to-surface are applied to bolt and segment.

Loading conditions. To obtain structural abnormal data, a concentrated force is applied on a local area of the tunnel arch crown. The concentrated force is linearly loaded onto the model until the load reaches 5000 kN. In addition, the loading mode and the position where the concentrated load is applied are shown in Fig. 4.

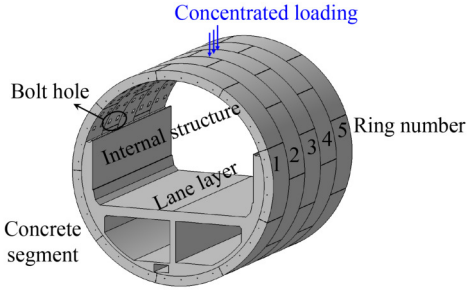

Fig. 3 Modeled tunnel structure.

Table 1 Property parameters of tunnel segment and bolt (EM stands for elasticity modulus)

Type	Material	Density (mm^{-3})	EM (MPa)	Poisson ratio
Segment	Concrete (C60)	2.4×10^{-9}	34500	0.2
Bolt	Steel	7.85×10^{-9}	210000	0.3

Table 2 Strain–stress data for a concrete segment

Stress (MPa)	Strain ($\times 10^{-3}$)
57.585	0.000
57.899	0.200
58.108	0.457
58.632	0.784
58.946	1.147
59.364	1.521
59.679	1.930
60.000	2.300
60.411	2.772
60.726	3.022

Constraint conditions. In the simulation phase, the rotational and translational freedoms in all directions are constrained. In fact, we mainly focus on the stress distribution on the middle ring (No. 3) although a five-ring model is developed, and the main role of the other rings in the simulation is to avoid the boundary effect. As an example, the stress variation trend of the concentrated load and the even load application locations are derived to analysis, as shown in Fig. 5. It can be found that stress at the position at which the concentrated force is applied is far larger than that at other positions. In addition, The location at which that force is applied variation trend deviates from that of other, which means some damages appear at the segment surface. After the above process, the structural abnormal data are constituted.

4.2 Data preprocessing for the experiment

If the stress variation of each element in which the load is applied is taken as a time series, the data set of the numerical result consists of 17422 time series, and each time series has 1000 records. In addition, 16859 time series store normal information, and 563 time series store structural abnormal information. Considering the single form of time series in the constructed data set, such that all abnormal data are caused by structural anomalies, it is necessary to construct some outliers caused by random factors. Therefore, Gaussian noises with different intensities are generated to pollute the numerical data set, where the pollution ratio is set to 10%. One of the polluted time series is selected randomly as an example, as displayed in Fig. 6. The data set including normal information, structural abnormal information, and random abnormal information is similar to the actual situation, so

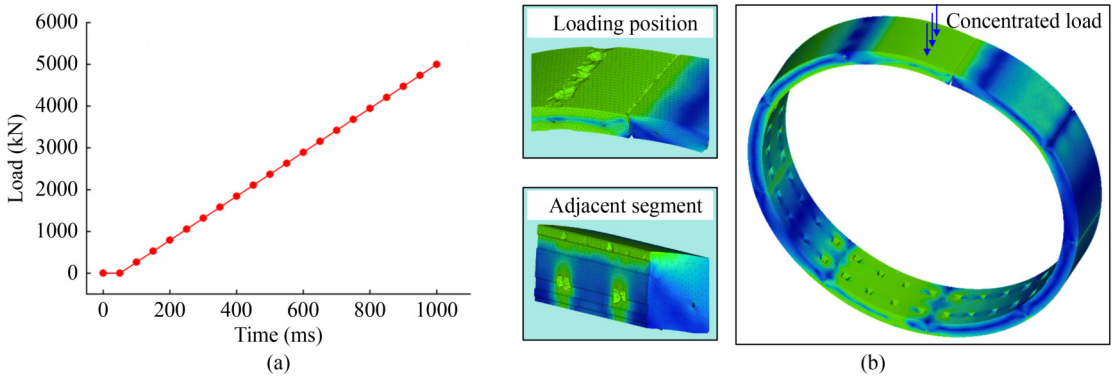

Fig. 4 Stress distribution of the middle segment: (a) loading mode; (b) loading position.

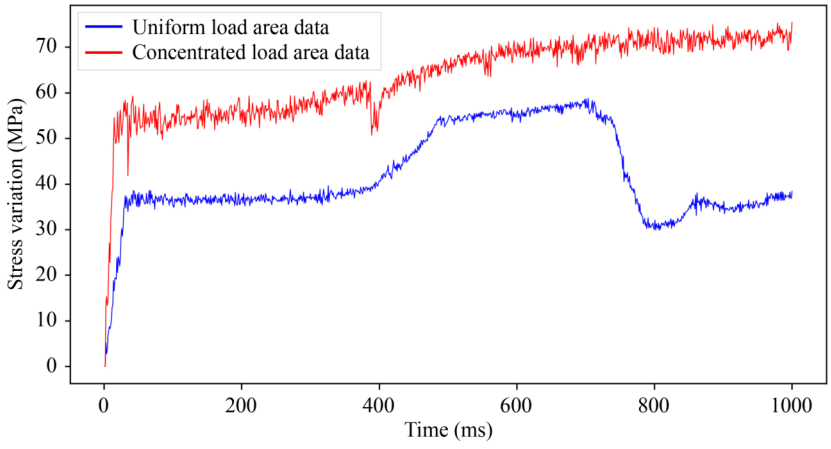

Fig. 5 Variation of stress with time.

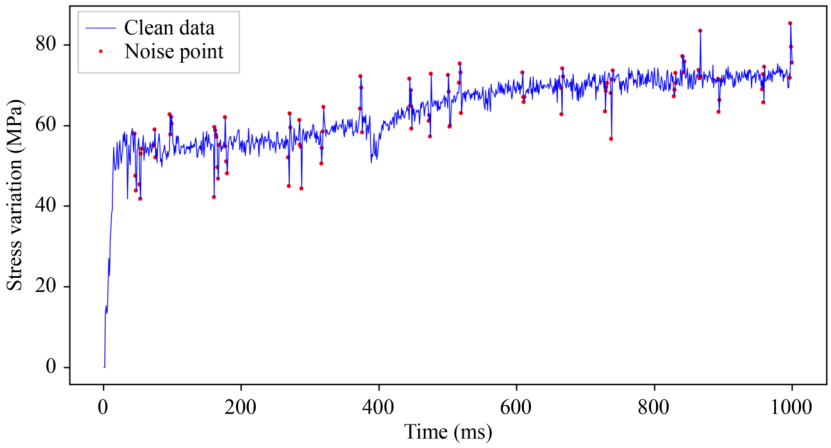

Fig. 6 Stress variation data polluted by the Gaussian noise.

the data set is suitable for conducting the anomaly detection experiment.

5 Data experiment according to devised model

In this section, experiments with field monitoring data obtained from the simulation system are conducted to verify the proposed model's effectiveness.

5.1 Experiment preparation

Before the data are input into the network, some preprocessing operations are needed.

There are 17422 feature points in the raw data set. For each feature point, we record 1000 moments of data at a frequency of 10000 Hz. Among the 17422 feature points, 563 points have abnormal moments. We choose these 563 points to verify our model's efficiency. To simulate noise pollution in real scenes, Gaussian noise, at a proportion of 10%, is added to the data set. The original data are in the form of long-range continuous time series, which is not suitable for neural networks. As mentioned in Subsection 2.1, we process the corrupted data into the form of sliding windows, and then feed them into the model. Taking sensor i, for example, the length of recorded time series of sensor i is T, and the sliding windows can be denoted as $w_k^i = \{\tilde{x}_k^i, \tilde{x}_{k+1}^i, \ldots, \tilde{x}_{k+W}^i\}, k = 1, 2, \ldots, T - W$, where W is the size of sliding window.

To reduce the impact of data distribution difference on anomaly detection, the Z-score normalization is applied. Taking μ to denote the mean value and σ to denote the standard deviation, the original input X will be transformed into

$$\tilde{X}^{\text{normal}} = \frac{\tilde{X} - \mu}{\sigma}. \tag{10}$$

5.2 Task setting

Our experiments are conducted under a computer environment with one Intel (R) Core (TM) i9-7900C CPU @ 3.30GHz and one NVIDIA Titan Xp GPU card. The noise generating mechanism is designed as a Gaussian function with sigma 1/2/4/8 superimposed on a sine function. Noise from 0 to 1 is randomly added to the original data to get the corrupted data. The size of the sliding window and the stride of the neural network are set as 12 and 1, respectively. The Encoder consists of two LSTM layers, and the size of the hidden state vector is 4. We train our model with Adam optimizer with a constant learning rate of 0.001, and use the mean squared error loss function as the objective function. Dropout with p = 0.1 is applied to the outputs of the Encoder and Decoder. We construct the training/validation/testing sets with a ratio of 7:1:2, and standardize the data before it is put into the network. The batch size is set to 4096. Early stop is performed by monitoring the validation error. In the testing phase, we search the cut-off value of maximum F1 Score (Subsection 5.3) on the validation set as the threshold, and then use this threshold to verify the effectiveness of the model on the testing set. The whole process can be complete in 20 min. The process of anomaly detection is shown in Algorithm 1.

5.3 Evaluation metrics

Considering that there are more normal samples than abnormal samples in the data set, we choose Accuracy (ACC), Precision (P), and F1 Score ($F1$) as evaluation metrics, and these are defined by:

$$ACC = \frac{TP + TN}{TP + TN + FP + FN}, \tag{11}$$

$$P = \frac{TP}{TP + FP}, \tag{12}$$

Algorithm 1: The process of anomaly detection

Data: Sequence of fragmented data $\mathbb{W} = \{\mathcal{W}^1, \mathcal{W}^2, \cdots, \mathcal{W}^I\}$, max epochs J, early stop epochs K;

Result: Random anomaly label y_r and structural anomaly label y_s;

Initialization: initialize all the parameters of f_{enc} and f_{dec};
$j \leftarrow 0, k \leftarrow 0, L'_{rec} \leftarrow +\infty, \hat{\mathcal{W}} \leftarrow \mathcal{W} + \epsilon$;
repeat
  Get $\tilde{\mathcal{W}}$ based on Eq. (7);
  Get L_{rec} based on equation Eq. (8);
  Update the parameters of f_{enc} and f_{dec} using L_{rec};
  $j \leftarrow j + 1$;
  if $L_{rec} < L'_{rec}$ then
    $k \leftarrow 0$;
    $L'_{rec} \leftarrow L_{rec}$;
  else
    $k \leftarrow k + 1$;
until $j = J$ or $k = K$;
$\mathcal{H} \leftarrow f_{enc}(\mathcal{W})$;
Get gauss $(\mathcal{H})$ based on Eq. (9);
Get random anomaly threshold δ_r and structural anomaly threshold δ_s. Refer to BeatGAN [37];
if gauss$(\mathcal{H}) < \delta_r$ then
  $y_r \leftarrow 1$;
else
  $y_r \leftarrow 0$;
if gauss$(\mathcal{H}) < \delta_s$ then
  $y_s \leftarrow 1$;
else
  $y_s \leftarrow 0$;

$$R = \frac{TP}{TP + FN}, \tag{13}$$

$$F1 = 2 \times \frac{P \cdot R}{P + R}. \tag{14}$$

where TP denotes for True Positives, FP denotes for False Positives, FN denotes for False Negatives, TN denotes for True Negatives. The higher the above evaluation metrics, the better the effectiveness of the model.

Considering that, in the field of civil engineering, it is of little significance to detect the anomaly at one-time point alone, we aggregate the 12 time points in an output window, and set the threshold as 5. In other words, if more than 4 anomalies are detected in the 12 time points, it is considered that the time period is abnormal.

5.4 Experimental results

Table 3 shows the performance of our proposed model on the SHMs data set. As shown in the table, the ability of our model to recognize anomalies is excellent. Even in the case of high noise intensity, the recognition ability of

Table 3 Experiment results of CIDAE

Metric	Sigma = 1	Sigma = 2	Sigma = 4	Sigma = 8
*F*1	0.8589	0.8562	0.8486	0.8344
P	0.8226	0.8121	0.8100	0.7851
ACC	0.9144	0.9119	0.9079	0.8976

the model is always good. As can be seen from Table 3, when the noise interference increases, the model's ability to identify structural anomalies decreases slightly. We hypothesize that with the increase of the noise, data distribution changes, the difference between normal and abnormal observations decreases, then it becomes more difficult for the model to extract robust features from the corrupted data. Nevertheless, the F1 score of our proposed model on the data set is always greater than 83%.

PCA is a commonly used data dimension reduction method. It can map high-dimensional data into low-dimensional space, while ensuring that low-dimensional vectors retain the features of high-dimensional data. We use PCA to map high-dimensional hidden state vectors to two-dimensional space and visualize them. The result of this visualization is shown in Fig. 7. As the figure shows, the normal points are distributed in the lower left corner of the canvas, and the distribution is clustered, while the abnormal points are relatively scattered in the other areas of the canvas. This indicates that the hidden state vectors already contain the effective characteristics of normal data and abnormal data, and can distinguish between them. We also note that as the intensity of noise increases, the distribution of normal points becomes sparse. That makes sense because noise with greater intensity will reduce the difference between normal points and abnormal points, and it becomes more difficult for the model to distinguish abnormal points from normal points. It also becomes more difficult to extract the robustness features of normal data. This is consistent with the experimental results shown in Table 3.

6 Verification and discussion

To demonstrate the superiority of the proposed model, some comparative experiments are conducted. As a case study, we test the effectiveness of CIDAE on Wuhan

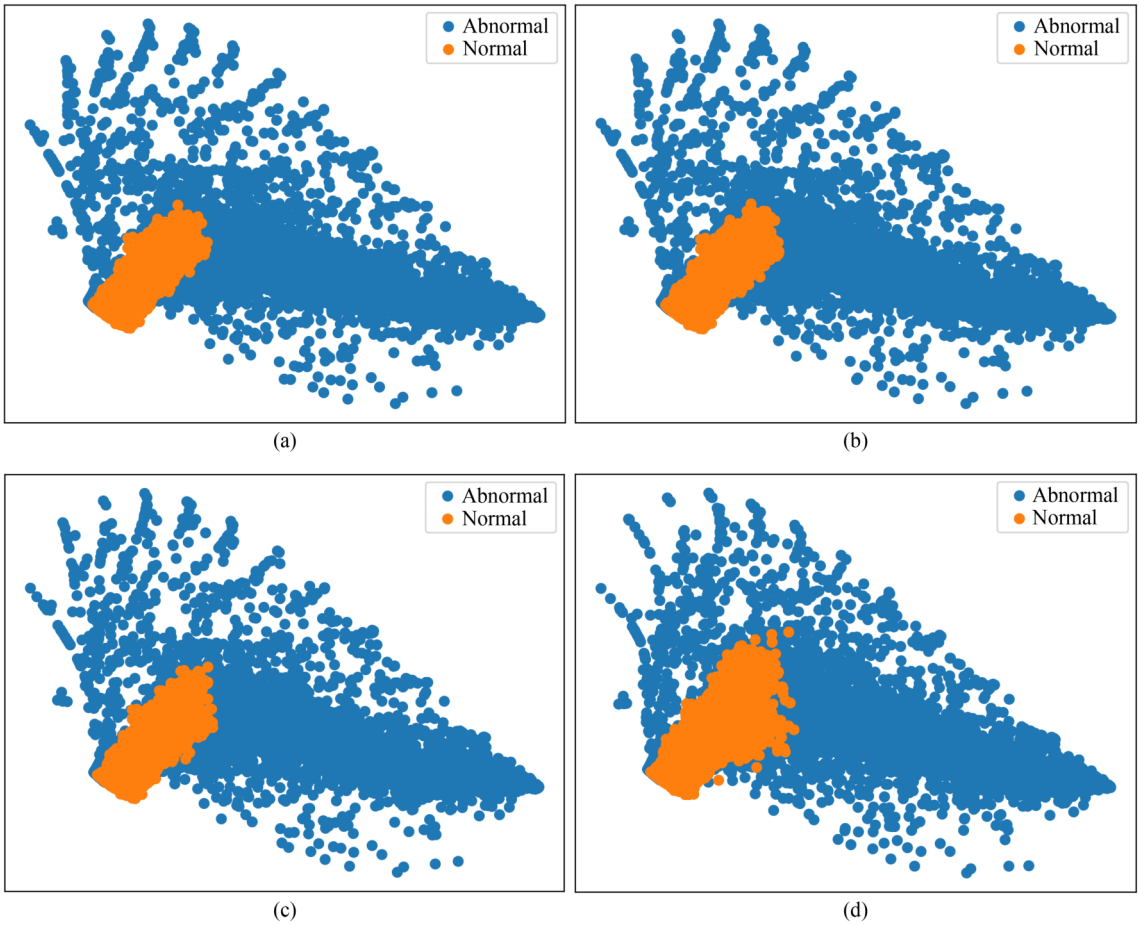

Fig. 7 Hidden state vector visualization based on PCA under different noise interference levels: (a) sigma = 1; (b) sigma = 2; (c) sigma = 4; (d) sigma = 8.

Yangtze River Tunnel.

6.1 Baselines

We take 3 unsupervised methods as our baselines.

Manual features extraction method (We use "feature" to refer to this model in Table 4). We extract the autocorrelation coefficient, mean, variance and standard deviation of each time period, and the vector composed of these four features is used to represent this series.

PCA [36]. This kind of method is based on matrix decomposition. By calculating the reconstruction error between the original matrix and the reconstructed matrix, the anomaly score can be defined.

AE [37]. This can be seen as a simplification of our approach. We retain the original structure of our proposed model, but we do not add noise to the input data.

6.2 Contrasting experiments with other methods

We conduct comparative experiments on noisy data with sigma 1, 2, 4, and 8. As Table 4 shows, our proposed model achieves the best results compared with other baselines. The manual features extraction method is the worst. This indicates that the feature information that can effectively represent time series cannot be extracted by ordinary feature extraction methods. The method based on matrix factorization can extract the information in the time series, but the AutoEncoder structure has stronger ability to extract the information. However, in noisy scenes, the method based on AE is prone to confuse abnormal samples with normal samples, which leads to overfitting and reduces the recognition ability of the model. CIDAE assigns lower weights to samples that look more abnormal during training, which makes the model more sensitive to anomalies. Even in the case of noisy input, the model can still effectively distinguish abnormal samples from normal samples.

6.3 Structural anomaly identification in a tunnel

The deformation stress data of the numerical underwater shield tunnel is based on a simulation experiment, so it is not practical data. In this section we verify the effectiveness of the proposed model on the longitudinal weld data and circumferential weld data of Wuhan Yangtze River Tunnel, which is a real data set. There are six joint sensors to record the variation of segment joint opening, and each sensor records a total of 2189 values, from September 11, 2013 to September 11, 2019, with a sampling frequency of once a day. The values recorded by the six sensors are shown in Fig. 8. The characteristics of the data are shown in Table 5, where sensor 1 to 3 record longitudinal weld data, and sensor 4 to 6 record circumferential weld data. The data set does not contain structural anomalies. We randomly select 10% of the data on the training set to be expand by 1.5 times of the original data, and these data are considered to represent structural anomalies. According to the characteristics of the data, we added Gaussian noise with standard deviations of 0.005, 0.01, 0.02, 0.04, and 0.08 to the training set, and we test the abnormal false positive rate of the models on the testing set. The data are normalized before feeding into the network to ensure that all features are expressed by values between 0 and 1. The other parameters of the model are the same as those introduced in Subsection 5.2. The accuracy of all methods is shown in Fig. 9. As shown in the figure, the proposed model achieves satisfactory results for all levels of noise disturbance. Compared with this, the accuracy rate of other methods is very low, indicating that CIDAE can accurately identify structural anomalies and noise disturbance, and avoid unnecessary false positives of anomalies. In general, with the increase of noise disturbance, the recognition accuracy of our model is further improved. It is speculated that the larger the disturbance intensity is, the more obvious the difference between noise and structural anomaly is, and it is easier for the model to distinguish between them.

7 Conclusions

This paper proposes a new scenario to identify civil infrastructure structural anomalies in noisy environments and offers a DAE-based anomaly detection model, CIDAE. Under the condition of unsupervised learning, CIDAE is used to eliminate the interference of noise on the model learning normal data distribution, extract the robust features of normal data, and improve the ability of the model to distinguish between normal data and abnormal data. Using the deformation stress data of the

Table 4 Overview performance of all methods

Metric	Sigma = 1			Sigma = 2			Sigma = 4			Sigma = 8		
	*F*1	*P*	*ACC*	*F*1	*P*	*ACC*	*F*1	*P*	*ACC*	*F*1	*P*	*ACC*
Feature	0.6011	0.4632	0.6709	0.5995	0.4721	0.6822	0.5528	0.4087	0.5997	0.5495	0.4069	0.5981
PCA	0.7303	0.6655	0.8269	0.7237	0.6493	0.8191	0.5387	0.5100	0.7168	0.5109	0.4503	0.6724
AE	0.8335	0.7727	0.8953	0.8290	0.7622	0.8914	0.7951	0.7107	0.8652	0.7922	0.7083	0.8634
CIDAE	0.8589	0.8226	0.9144	0.8562	0.8121	0.9119	0.8486	0.8100	0.9079	0.8344	0.7851	0.8976

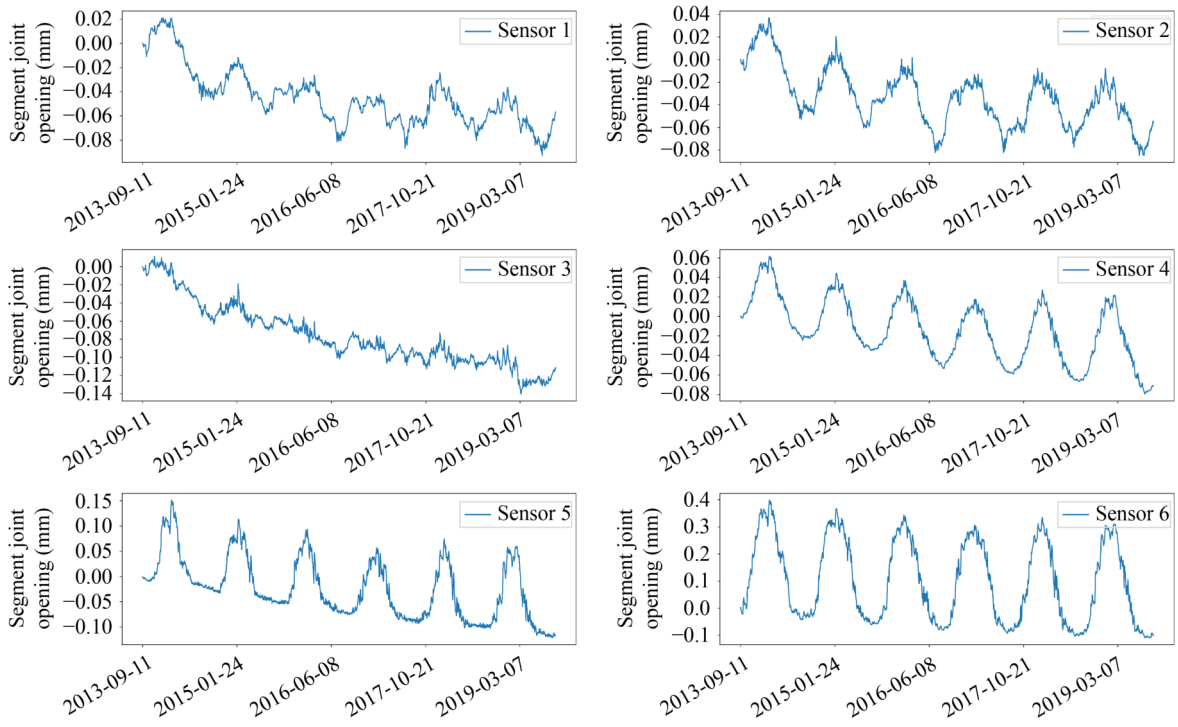

Fig. 8 Monitoring data recorded by six joint sensors.

Table 5 Characteristics of circumferential weld and longitudinal weld data

Sensor ID	Minimum (mm)	Maximum (mm)	Mean (mm)	Standard deviation (mm^2)
1	−0.0926	0.0211	−0.0451	0.0006
2	−0.0848	0.0369	−0.0337	0.0007
3	−0.1404	0.0112	−0.0761	0.0012
4	−0.0796	0.0615	−0.0140	0.0010
5	−0.1213	0.1511	−0.0228	0.0036
6	−0.1089	0.3984	−0.1009	0.0224

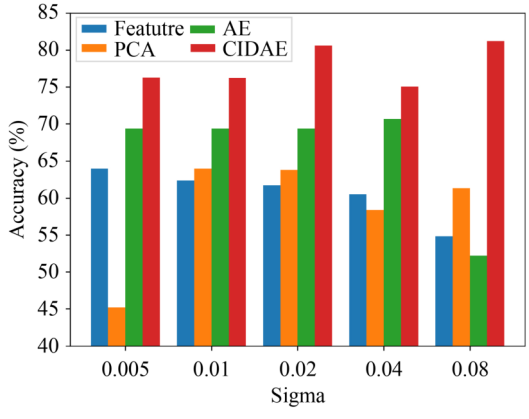

Fig. 9 Overall performance of all methods on circumferential weld and longitudinal weld data.

Wuhan Yangtze River Tunnel based on the finite element simulation model to carry out experiments, adding compound noise to the simulation data, the accuracy rate of the model identifying structural anomalies is always above 89%, the precision rate is above 78%, and the $F1$ Score is above 83%. These values verify the effectiveness of the proposed model. The comparative experiments prove the superiority of the proposed model compared with other feature extraction models. Experiments on the real data set of circumferential weld and longitudinal weld data of the Wuhan Yangtze River Bridge prove that, unlike the traditional methods, the model does not produce abnormally high false positives. Compared with traditional methods, the deep learning method CIDAE proposed in this paper can accurately identify civil infrastructure structural anomalies in the presence of noise interference, and is suitable for applications in real engineering cases.

At present, many works have studied the anomaly identification problem in the field of civil infrastructure health detection, but have been limited by the ability of the model, so that few works have considered the widespread existence of noise in real engineering scenarios. This paper proposes a new approach to identification of meaningful civil infrastructure structure anomaly where there is noise interference. In addition, an unsupervised deep learning method that can be used for anomaly identification is proposed, which provides inspiration for researchers. In future work, more attention should be paid to unsupervised anomaly recognition methods in real complex scenes to adapt to applications in real scenarios.

Acknowledgements This work was supported by the National Natural Science Foundation of China (Grant Nos. 51991395, 51991391, and U1811463) and the S&T Program of Hebei, China (No. 225A0802D).

Competing interests The authors declare that they have no competing interests.

References

1. Bado M F, Casas J R. A review of recent distributed optical fiber sensors applications for civil engineering structural health monitoring. Sensors, 2021, 21(5): 1818–1901
2. Bao Y, Li H. Machine learning paradigm for structural health monitoring. Structural Health Monitoring, 2021, 20(4): 1353–1372
3. Chen J, Jiang X, Yan Y, Lang Q, Wang H, Ai Q. Dynamic warning method for structural health monitoring data based on arima: Case study of Hong Kong–Zhuhai–Macao bridge immersed tunnel. Sensors, 2022, 22(16): 6185–6202
4. Hou R, Xia Y. Review on the new development of vibration-based damage identification for civil engineering structures: 2010–2019. Journal of Sound and Vibration, 2021, 491: 115741
5. Chen H P. Structural Health Monitoring of Large Civil Engineering Structures. CSU Academic Report, 2018
6. Entezami A, Sarmadi H, Saeedi Razavi B. An innovative hybrid strategy for structural health monitoring by modal flexibility and clustering methods. Journal of Civil Structural Health Monitoring, 2020, 10(5): 845–859
7. Cao P, Qi S, Tang J. Structural damage identification using piezoelectric impedance measurement with sparse inverse analysis. Smart Materials and Structures, 2018, 27(3): 035020
8. Moore E Z, Nichols J M, Murphy K D. Model-based SHM: Demonstration of identification of a crack in a thin plate using free vibration data. Mechanical Systems and Signal Processing, 2012, 29: 284–295
9. Xu L, Wang K, Yang X, Su Y, Yang J, Liao Y, Zhou P, Su Z. Model-driven fatigue crack characterization and growth prediction: A two-step, 3-d fatigue damage modeling framework for structural health monitoring. International Journal of Mechanical Sciences, 2021, 195: 106226
10. Malekloo A, Ozer E, AlHamaydeh M, Girolami M. Machine learning and structural health monitoring overview with emerging technology and high-dimensional data source highlights. Structural Health Monitoring, 2022, 21(4): 1906–1955
11. Mosavi A A, Dickey D, Seracino R, Rizkalla S. Identifying damage locations under ambient vibrations utilizing vector autoregressive models and Mahalanobis distances. Mechanical Systems and Signal Processing, 2012, 26: 254–267
12. Xiao S, Li S. LSSVM-based approach for refining soil failure criteria and calculating safety factor of slopes. Frontiers of Structural and Civil Engineering, 2022, 16(7): 871–881
13. Tibaduiza D, Torres-Arredondo M A, Vitola J, Anaya M, Pozo F. A damage classification approach for structural health monitoring using machine learning. Complexity, 2018, 5081283
14. Sheikh Khozani Z, Khosravi K, Torabi M, Mosavi A, Rezaei B, Rabczuk T. Shear stress distribution prediction in symmetric compound channels using data mining and machine learning models. Frontiers of Structural and Civil Engineering, 2020, 14(5): 1097–1109
15. Mai H V T, Nguyen M H, Trinh S H, Ly H B. Optimization of machine learning models for predicting the compressive strength of fiber-reinforced self-compacting concrete. Frontiers of Structural and Civil Engineering, 2023, 17(2): 284–305
16. Wang Z, Cha Y J. Unsupervised machine and deep learning methods for structural damage detection: A comparative study. Engineering Reports, 2022, e12551
17. Ye X W, Jin T, Yun C B. A review on deep learning-based structural health monitoring of civil infrastructures. Smart Structures and Systems, 2019, 24(5): 567–585
18. Jansen A, Geißler K. Multi-feature anomaly detection for structural health monitoring of a road bridge using an autoencoder. In: 10th International Conference on Structural Health Monitoring of Intelligent Infrastructure–SHMII. 2021, 10
19. Moallemi A, Burrello A, Brunelli D, Benini L. Model-based vs. data-driven approaches for anomaly detection in structural health monitoring: A case study. In: Proceedings of 2021 IEEE International Instrumentation and Measurement Technology Conference (I2MTC). New York: IEEE, 2021
20. Shu X, Bao T, Zhou Y, Xu R, Li Y, Zhang K. Unsupervised dam anomaly detection with spatial-temporal variational autoencoder. Structural Health Monitoring, 2023, 22(1): 39–55
21. Cha Y J, Choi W, Büyüköztürk O. Deep learning-based crack damage detection using convolutional neural networks. Computer-Aided Civil and Infrastructure Engineering, 2017, 32(5): 361–378
22. Chiaia B, Marasco G, Aiello S. Deep convolutional neural network for multi-level non-invasive tunnel lining assessment. Frontiers of Structural and Civil Engineering, 2022, 16(2): 214–223
23. Bao Y, Tang Z, Li H, Zhang Y. Computer vision and deep learning-based data anomaly detection method for structural health monitoring. Structural Health Monitoring, 2019, 18(2): 401–421
24. Huang H B, Yi T H, Li H N. Anomaly identification of structural health monitoring data using dynamic independent component analysis. Journal of Computing in Civil Engineering, 2020, 34(5): 04020025
25. Wang Z, Cha Y J. Unsupervised deep learning approach using a deep auto-encoder with a one-class support vector machine to detect damage. Structural Health Monitoring, 2021, 20(1): 406–425
26. Cha Y J, Wang Z. Unsupervised novelty detection-based structural damage localization using a density peaks-based fast clustering algorithm. Structural Health Monitoring, 2018, 17(2): 313–324
27. Favarelli E, Testi E, Giorgetti A. The impact of sensing parameters on data management and anomaly detection in structural health monitoring. Journal of Civil Structural Health Monitoring, 2022, 12(6): 1–13
28. Yan S, Shao H, Xiao Y, Liu B, Wan J. Hybrid robust convolutional autoencoder for unsupervised anomaly detection of machine tools under noises. Robotics and Computer-integrated Manufacturing, 2023, 79: 102441
29. Mostafavi A, Cha Y J. Deep learning-based active noise control on construction sites. Automation in Construction, 2023, 151: 104885
30. Cha Y J, Mostafavi A, Benipal S S. Benipal. Dnoisenet: Deep

learning-based feedback active noise control in various noisy environments. Engineering Applications of Artificial Intelligence, 2023, 121: 105971

31. Krasichkov A S, Grigoriev E B, Bogachev M I, Nifontov E M. Shape anomaly detection under strong measurement noise: An analytical approach to adaptive thresholding. Physical Review E: Statistical, Nonlinear, and Soft Matter Physics, 2015, 92(4): 042927
32. Raginsky M, Willett R M, Horn C, Silva J, Marcia R F. Sequential anomaly detection in the presence of noise and limited feedback. IEEE Transactions on Information Theory, 2012, 58(8): 5544–5562
33. Vincent P, Larochelle H, Bengio Y, Manzagol P A. Extracting and composing robust features with denoising autoencoders. In: Proceedings of the 25th international conference on Machine learning. New York: ACM, 2008, 1096–1103
34. Tan X, Chen W, Tan X, Zou T, Du B. Prediction for the future mechanical behavior of underwater shield tunnel fusing deep learning algorithm on shm data. Tunnelling and Underground Space Technology, 2022, 125: 104504
35. Zhou B, Liu S, Hooi B, Cheng X, Ye J. Beatgan: Anomalous rhythm detection using adversarially generated time series. In: Proceedings of IJCAI-19. San Mateo: IJCAI, 2019, 4433–4439
36. Hotelling H. Analysis of a complex of statistical variables into principal components. Journal of Educational Psychology, 1933, 24(6): 417–441
37. Rumelhart D, Hinton G E, Williams R J. Learning representations by back-propagating errors. Nature, 1986, 323(6088): 533–536